

EARLY ONLINE RELEASE

This is a PDF of a manuscript that has been peer-reviewed and accepted for publication. As the article has not yet been formatted, copy edited or proofread, the final published version may be different from the early online release.

This pre-publication manuscript may be downloaded, distributed and used under the provisions of the Creative Commons Attribution 4.0 International (CC BY 4.0) license. It may be cited using the DOI below.

The DOI for this manuscript is

DOI:10.2151/jmsj.2022-024

J-STAGE Advance published date: February 3rd, 2022

The final manuscript after publication will replace the preliminary version at the above DOI once it is available.

Tropical Cyclones Affecting Japan Central Coast and Changing Storm Surge Hazard since 1980

Md. Rezuatul ISLAM¹

*School of Environment and Society
Tokyo Institute of Technology, Tokyo, Japan*

Masaki SATOH

*Atmosphere and Ocean Research Institute
The University of Tokyo, Tokyo, Japan*

and

Hiroshi TAKAGI

*School of Environment and Society
Tokyo Institute of Technology, Tokyo, Japan*

January 19, 2022

1) Corresponding author: Md. Rezuatul Islam, School of Environment and Society, Tokyo Institute of Technology, 2 Chome-12-1 Ookayama, Meguro City, Tokyo 152-8550 JAPAN
Email: fahiemislam@gmail.com
Tel: +81-070-3516-3635

Abstract

This study investigated tidal records and landfall tropical cyclone (TC) best tracks from 1980 to 2019 to determine changes in storm surge heights in coastal regions of Central Japan, including Tokyo. The results indicate that annual mean storm surge heights have increased in the last 20 years (2000–2019) compared to those in 1980–1999, and that these changes are noteworthy, particularly in Tokyo Bay. TC wind intensity and size during landfall time frame have become stronger and larger, respectively, corresponding to increasing storm surge magnitudes from 1980 to 2019. The increased occurrence frequency of TCs with more northeastward tracks is another factor that may have contributed to the increased surge hazards around Tokyo. Additionally, a positive correlation between surge heights and a hazard index supports these statistical findings. Japan central coast will likely experience increasing numbers of extreme storm surge events in the future, if, the current increasing tendency continues.

Keywords tropical cyclone; storm surge; trend analysis; surge hazard potential index; Tokyo;

1. Introduction

Tropical cyclone (TC)-generated storm surge is one of the most deadly and costly global hazards. In the last two decades, Hurricane Katrina (2005), Cyclone Sidr (2007), Cyclone Nargis (2008), and Typhoon Haiyan (2013) have each caused more than 1,000 fatalities, many of which were the direct result of storm surges (Esteban et al. 2015). Although extreme storm surges do not occur often, the related damage and impacts can be enormous in densely populated urban areas. For example, Hurricane Sandy (2012) inflicted a catastrophic storm surge of ~2.7 m and resulted in USD 50 billion losses, particularly from storm surge along the mid-Atlantic coast, including the New York City metropolitan area (Blake et al. 2013). Typhoon Jebi in 2018 caused an inundation in Osaka Bay, Japan, and the Kansai-Osaka International Airport was entirely inundated, which resulted in USD 2 billion in damages (Anh et al. 2019). Recent studies have suggested that the number of residents in coastal urban areas and the number of individuals exposed to flooding from once in 100-year storm surge events will continue to increase in the future (Nicholls and Cazenave 2010; Brown et al. 2013; Hallegatte et al. 2013; Neumann et al. 2015). Therefore, it is of great importance to understand whether any changes in storm surge hazards affecting large cities have occurred in recent years, despite the relatively infrequent occurrence of major storm surge events.

Analyzing the changes in storm surge trends in a certain location helps to assess whether coastal flooding risk reduction efforts are effective. Therefore, previous studies have

analyzed changes in historical surge magnitudes in a specific location or globally. Several of these studies have concluded that surge levels are increasing over time. For example, Woodworth and Blackman (2004) and Menéndez and Woodworth (2010) analyzed storm-induced abnormal sea-level changes by using a global tide gauge dataset. They concluded that many of the gauges showed significant increases in abnormal sea levels since 1970. Bromirski et al. (2003) found a significant increasing trend in extratropical surges in San Francisco since 1950. Church et al. (2006) observed an increase in the frequency of high-water levels (storm surges plus mean sea-level rise) after 1950 by using data from two tide gauges on the eastern and western Australian coasts. These studies have confirmed that mean sea-level rise, interannual, and decadal variations are the main factors contributing to the increase in maximum surge height. However, changes in TC characteristics such as intensity, track, size, and translation speed are also capable of modulating the surge hazard potential. For example, Irish et al. (2008) evaluated the relationship between TC size (radius to maximum wind speed) and maximum storm surge over idealized continental shelf slopes. Their results demonstrated that storm surges tend to increase with TC size and that this relationship becomes increasingly pronounced for shallow coastal waters. Regarding the effect of TC translation speed on storm surge, an investigation of the Louisiana–Texas coasts (US) by Rego and Li (2009) revealed that slower TCs (with a translation speed of 12.6–18.0 km/h) cause more extensive flooding, while faster TCs produce higher surges but with comparatively less flood volume. Sebastian et al. (2014) found that storm surge

behavior in a small water basin, such as Galveston Bay (US), is highly sensitive to the local wind direction associated with TC landfall location. These findings support the conclusion of our recent work (Islam and Takagi 2020a), in which we showed that storm surge characteristics in a semi-enclosed bay, such as Tokyo Bay in Japan, is largely sensitive to the landfall location, local wind direction, translation speed, and storm size. Therefore, assessing whether TC meteorological parameters influence storm surge hazards over time at a specific location is also necessary. Specifically, this allows us to investigate the association between temporal variations of surge hazards and surge sensitive TC meteorological parameters including intensity, size, translation speed, and track.

The Western North Pacific (WNP) basin is the most active area on the Earth for TCs, as approximately one-third of the world's TCs develop in the region (Elsner and Liu 2003). The WNP basin includes the greater Tokyo area, Central Japan (34° – 36° N, 137° – 141° E; Fig. 1), which is one of the largest and busiest coastal urban areas in the world (United Nations 2018), where TC-induced storm surge poses a considerable threat to millions of coastal inhabitants (Islam et al. 2018). Swiss Re (2013) ranked 616 cities worldwide in terms of their potential risks for natural disasters, including TCs and storm surges, and reported that the Greater Tokyo Area is subject to the highest risks. Although the TC landfall frequency is not very high in Central Japan compared to that of southwestern Japan (Islam and Takagi 2020a), strong TCs sometimes reach Japan Central Coast, causing billions of dollars in damage to the infrastructure (JMA 2020a). Among the major TCs that have directly affected

this region over the past century, a TC in 1917 (known locally as Typhoon Taisho) was the most devastating. The storm surge induced by this typhoon claimed 1,301 lives, destroyed 43,083 houses, and swept away 8,220 marine vessels (Omori 1918). In modern times, most of the coastal areas of Japan including those of Central Coast are protected from storm surges by coastal dikes. However, their design heights have not necessarily been adequately designed because of short period of tidal observations (Torii and Kato 2004). In addition, the coastal embankment in the bay (i.e., Tokyo Bay) did not sufficiently consider high waves caused by a rare but strong TC, and the structural design height tends to be underestimated (Takagi and Takahashi 2021). Thus, there is an uncertainty regarding whether urban waterfronts of Tokyo and its neighboring cities are sufficiently resilient against future powerful TCs (Islam et al. 2018). Concerns about TCs and storm surge impacts have considerably increased among the local population since Typhoon Faxai and Typhoon Hagibis hit the Greater Tokyo Area in 2019. These two typhoons caused severe coastal damage and were classified as the strongest typhoons since the JMA typhoon database was created in 1951 (Shimozono et al. 2020; Takagi et al. 2020). Yamaguchi and Maeda (2020a) showed that the number of TCs, including stronger storms approaching the central coast of Japan, including Tokyo, has a decadal increasing trend since 1980. They also determined that the translation speeds of TCs have decreased from 1980 to 2019, which indicates that Tokyo and its surroundings experienced TC influences of a longer duration over time (Yamaguchi and Maeda 2020b). These recent studies and TC events raise

questions as to whether the magnitude of the storm surge that has affected Tokyo and its neighboring cities has increased recently and whether changes in the storm surge hazard potential are larger than previously determined. Currently, there is no study that has examined long-term storm surge observations and factors that influence surge hazards in Japan central coast.

This study examines changes in storm surge hazards in Japan central coast since 1980 in terms of temporal variations in storm surge heights and statistically investigates factors that influence surge magnitudes. We also inspected changes in the TC tracks and their potential influence on storm surge variations. We used tidal records from ten tide stations and best track information for TCs that made landfall around the central coast of Japan. As a secondary objective, we also investigate the applicability of a storm surge index, SSHPI, proposed by Islam et al. (2021) in this region.

2. Data and Methods

In this study, we considered a period spanning from 1980 to 2019 and obtained TC best track data from the Japan Meteorological Agency (JMA) archives, including data pertaining to TCs that originated in the WNP and made landfall around the central coast of Japan (JMA 2020a). The best track data acquired during the pre-satellite era (i.e., before 1980) contain heterogeneities and large uncertainties in data quality (Chan 2019; Moon et al. 2019) and therefore were ignored. Although the time period processed was relatively short, the period

of 1980–2019 was the longest period covered by the JMA best track dataset that has uniform data quality. Data collection was limited to TCs with a maximum sustained wind speed (V_{max}) of greater than 17 m s^{-1} (33-kt) made landfalls in Japan central coast. This target area is bounded in latitude by 34°N and 37°N , and longitude by 137°E and 141°E (Fig. 1). It includes major coastal cities including Tokyo, Yokohama, Chiba, Hamamatsu, Shizuoka, Shimoda, Katsura, and Choshi. Adopting wind intensity threshold is required because TCs are not always powerful (i.e., tropical depressions) and may not produce noticeable storm surge; thus, it would be more meaningful to focus on tropical storms ($34\text{-kt} \leq V_{max} \leq 63\text{-kt}$) or stronger TCs (i.e., category 1, 2 in Saffir-Simpson Hurricane Wind Scale) for disaster risk management. Based on these criteria, 36 TCs were selected for analysis (Fig. 1). These TCs were further divided into two categories based on their landfall locations: open coastlines (directly facing the Pacific Ocean) and bay areas (regions surrounded by two land areas that form a concave section of coastline). Of the 36 TCs, 10 made landfalls on open coastlines. The remaining 26 TCs made landfalls between open coastlines and bay areas and affected both regions. Among the 36 TCs, 19 and 12 TCs impacted more than one tidal station located on the open coastlines and bay areas, respectively. As a result, there were 72 and 90 available storm surge cases for open coasts and bay areas, respectively, for a total of 162 cases.

We analyzed best track TC central positions, intensities, sizes, and translation speeds at the landfall time frame (T) because storm surge tends to be amplified at the time of landfall.

However, TC characteristics during the landfall time frame are not necessarily the most adverse condition to cause the largest storm surge on coasts. For example, storm surges would take the largest value when the TC track is closer to the bay. In this study, we considered TC landfall time rather than the time closest to each tide station as a representative condition for causing peak surge because, (a) TC characteristics (i.e., intensity, size, translation speed), after landfall, differ from those over the ocean. Thus, the TC information over land is considered less reliable (Huang et al. 2021); (b) Although the recent TC best track contains more detailed information about when a TC approaches the land, the JMA best track historically has provided TC information at every 6 h intervals. It is difficult to identify the time of closest approach to a station with the 6 h interval data; (c) In the current dataset, 26 of 36 TCs affected both open coasts and bays, and storm surge information was recorded for more than one tidal station for those TCs. Thus, a unique characteristic (i.e., landfalling TC intensity) for each storm can provide a simple basis for statistical analysis.

According to the JMA (2020b), TC landfall is identified when the center of a TC reaches the coastline of the mainland (Honshu, Hokkaido, Kyushu, Shikoku) in Japan. We detected the approximate landfall point at which a TC track intersects a coastline by using a vector data provided by the Geospatial Information Authority of Japan (2021). Figure 2 shows TC landfall points ($n = 36$) along the coasts of central Japan. The translation speed at time T ($T =$ landfall time frame) was calculated using the TC central positions at T and $T - 6$ h. Among the 36

TCs, translation speed, intensity, and size data for six TCs were not available at T . Hence, estimations for the six TCs were obtained via linear interpolation of the available data from immediately before and after landfall. The bathymetry of the target region was obtained from the Japan Oceanographic Data Center (JODC), Japan Coast Guard (JODC 2020a).

Figure 3 shows the ten JMA and Japan Coast Guard-operated tidal stations (JMA 2020c; JODC 2020b) used to estimate the peak storm surge for each TC. However, it needs to be noted that observed tidal records are hourly, thus, surge records used in this study are not necessarily exact peak values. Among many operational stations, data collection was limited to those that satisfied the five criteria: (a) fell to the right side of a selected TC track and located within the range of radius of 50-kt wind (R_{50} ; during TC landfall time frame); (b) located on an open coastline or in a bay. Stations on islands were excluded; (c) JMA predicted astronomical tide data were available (JMA 2020d); (d) elevations of the observation reference plane and the astronomical tide table reference plane were available; and (e) no data gaps occurred when a TC traversed over the station. Five stations were selected from open coastlines (Maisaka, Omaezaki, Irouzaki, Mera, and Choshi), and five stations were selected from semi-enclosed bays (Shimizuminato, Uchiura, Yokohama, Tokyo, and Chiba). Figure 3 provides details of the selected tidal stations. Notably, wave set-up is often the dominant driver for generating storm surge in some selected tidal stations (e.g., Omaezaki, Irouzaki, and Mera); however, this influence was not considered, to keep the analysis simple. Sea surface anomalies were defined as the storm surge magnitude (in

cm in this study) and were estimated by deducting the predicted astronomical tide from the observed storm tide.

TC-induced annual storm surge hazard potential at T (T = landfall time frame) was calculated to demonstrate how the factors influencing storm surge hazard potentials have changed over the last 40 years. It was estimated for all TCs by using the storm surge hazard potential index (SSHPI, Islam et al. 2021). The SSHPI incorporates meteorological information sensitive to storm surge, including TC intensity, size, and translation speed, along with coastal geometry (open coasts and bays) and regional scale bathymetry into a single measure of the expected surge hazard potential along the coast. The effectiveness of the SSHPI for predicting peak surge hazard potential were discussed in Islam et al. (2021). Detailed definition of SSHPI is described in Appendix. TC best track data were used to calculate the SSHPI for each storm. Table 1 shows the predictors used in the SSHPI calculation. TC conditions at T were used to estimate SSHPI; therefore, it does not necessarily indicate adequate storm surge heights especially when landfall points are far from the selected tidal stations.

The storm surge and surge hazard potential time series were calculated based on annual mean storm surge heights and annual mean SSHPIs from 1980 to 2019. We divided the 40-year dataset into two sub-periods: 1980–1999 and 2000–2019, hereafter referred to as P1 and P2, respectively. The temporal changes in storm surge height and SSHPI were estimated by linear regression. The percentage change was calculated by dividing the

difference between the last and first points of the best-fit line by the first point. The two-tailed Student's *t*-test was used to determine if the means of any two sets of data were significantly different. The *p*-values of the regressions and *t*-test statistics were calculated based on the two-tailed 95% confidence level test.

3. Results

3.1 Observational evidence

The time series of annual mean storm surge heights is shown in Fig. 4a. A highly significant increase in storm surge height of +41% occurred per decade from 1980 to 2019. Annual mean storm surges of 24 cm and 55 cm occurred in Japan central coast in P1 and P2, respectively. The difference between the periods is statistically significant at the 95% level. A similar increasing tendency (+40% per decade from 1980 to 2019) was also observed for the dataset comprising annual peak storm surge heights (Fig. 4b). At least one storm surge event with a peak surge height of ~100 cm occurred annually since 2011 in Central Japan. In terms of the criteria considered in this study (see Section 2 for the definition of the TC landfall), P1 contained 11 years when no identifiable storm surge occurred in Central Japan (1980, 1982, 1984, 1986, 1987, 1988, 1992, 1994, 1995, 1996, and 1999). In contrast, P2 contained only four years without a storm surge occurrence (2003, 2006, 2008, and 2010). Such differences in the TC landfall frequency appear to contribute to a larger storm surge tendency in P2 than in P1. However, a significant change was also evident in the years with

storm surge events. To test the robustness of the statistics presented herein, particularly the outliers, the results were reaffirmed using the L^1 norm (not shown) in place of the ordinary least-squares (L^2) norm. A slight change was observed, but none of the significant changes from the L^2 regression became insignificant.

The distribution of storm surge events exhibited a clear shift towards greater heights during P2, and the differences were significant throughout most of the distribution (Fig. 5). For example, there was a significantly higher probability of larger storm surges >95 cm during P2, whereas a significantly higher probability of smaller storm surges <65 cm during P1. In other words, the occurrence frequency of significant storm surges (i.e., >95 cm) in the study area increased in P2 (eight times) than in P1 (two times). It needs to be noted that the present analyses are limited for the specified target area, if storm surge information for other regions were included, surge characteristics for central Japan coast could be different.

3.2 Spatial distribution of storm surge statistics

Figure 6 shows the spatial distribution of storm surge statistics between P1 and P2 at the ten tidal stations. While an overall increase in storm surge height was evident at all stations, a statistically increasing tendency was more pronounced at four stations (Harumi, Chiba, Yokohama, and Mera) in Tokyo Bay. The magnitude of the change indicates that storm surge heights in Tokyo Bay increased by an average of +45% per decade, which is 4% larger than the overall increase (+41%) observed along the central Japan coasts, including Tokyo and its' neighboring cities (considering all ten stations). Only one case shows the storm surge

exceeded 100 cm in Tokyo Bay during P1, in contrast with six events recorded during P2, including four events in the last 10 years. Additionally, similar significant increases in storm surge heights were evident along open coasts (+33% per decade; considering five stations on open coastlines) and in semi-enclosed bays (+44% per decade; considering five stations in bays).

3.3 Changes in TC parameters influence storm surge

Table 2 shows the differences in the TC parameters that can influence surge magnitude, including wind speed, TC size, and translation speed at the landfall time, between P1 and P2. TCs during P2 had more influences on greater storm surge generation than those in P1 due to stronger wind speeds and larger sizes. Differences in wind speed and size between P1 and P2 were statistically significant at the 95% level. Although landfalling TC translation speeds during P2 decreased by ~5% compared with P1, this difference was not statistically significant. This finding was in contrary to the findings of Yamaguchi and Maeda (2020b), who found a significant decrease (36%) in the translation speed of approaching TCs in Japan central coast. However, Yamaguchi and Maeda's (2020b) findings were valid for the selected approaching TCs (including those that did not make landfall) in September over the last 40 years (1980-2019). In this study, we considered all the TCs that made landfall in any month (the selected 36 TCs made landfall between June to October) during the same 40-year period.

Figure 7 shows the occurrence frequency of the TCs that made landfalls in central Japan

coast as a function of their wind intensities, sizes, and translation speeds at the time of landfall. Note that the occurrence frequency is not equal to the total number of TCs. This observation indicated that the number of landfalling TCs that fulfilled the criteria used in this study ($n = 36$; see section 2, Data and Methods for the selection of TC). The numbers of occurrence frequencies of TCs with $V_{max} > 60$ -kt during P1 and P2 were 0.15 and 0.75 per year, respectively (Fig. 7a). Thus, there were five times more chances for a TC to affect central Japan during P2 than during P1, i.e., the frequency of strong TCs has increased over time. This finding is consistent with those of Yamaguchi and Maeda (2020a), who found that the frequency of strong TCs with a central pressure <980 hPa that approached central Japan coast increased by 2.5 times. Figure 7b shows that the numbers of occurrence frequencies during P1 and P2 in the $R_{50} \leq 40$ NM bin were 0.3 and 0.35 per year, respectively. In contrast, TCs with $R_{50} > 70$ NM had five times more chance of affecting Japan central coast during P2 compared with P1. No clear changes in frequency were observed in terms of TC translation speed during the last 40 years (Fig. 7c). It needs to be noted that the statistics presented in Fig. 7 are based on low- frequency TC events (lower than one per year); therefore, the likelihood of overestimation or underestimation is not negligible.

4. Discussion

4.1 Changes in storm surge hazard potential

The purpose of this study was to determine whether there have been significant changes in the storm surge hazards in Japan Central Coast in the last 40 years by examining TC parameters that can influence the surge hazard in addition to the storm surge magnitudes. We have shown that surge sensitive TC parameters including intensity and size have changed from 1980 to 2019 in the previous section. In particular, it is important to quantify the contribution of those parameters on the increasing surge magnitude as shown in Section 3. Therefore, we applied SSHPI (Islam et al. 2021) to demonstrate the statistical sensitivity of each TC parameter in changing surge hazards.

Figure 8 shows the annual mean SSHPIs at the time of TC landfall and the annual mean storm surge heights for Japan central coast. SSHPI constitutes surge sensitive TC meteorological parameters; thus, it can be used to quantify the hazardous surge events by varying the parameters. The correlation coefficient of 0.825 indicates a strong positive correlation between annual mean SSHPI and annual mean storm surge height. This result supports the analysis by Islam et al. (2021), in which SSHPI was strongly correlated with actual surge heights observed throughout Japan. The SSHPI time series exhibited an evident increase of +61% per decade from 1980 to 2019 which has a similarity with the decadal storm surge increasing (+41%) tendency. It needs to be noted that SSHPI underestimated observed surges in P1 which caused the difference in overall increasing tendency by SSHPI than that of observed storm surges. A similar increasing tendency was observed for both the open coastlines and semi-enclosed bays (not shown). Annual mean

SSHPIs of 0.21 and 0.71 were obtained for P1 and P2, respectively. The difference between these SSHPIs is statistically significant at the 95% level, indicating that the increase in the SSHPI during P2 is unusual with the large upswing in surge heights observed particularly in the last decade (2010-2019). This increase in the SSHPI and surge height may result from the more intense and larger TCs during this period.

There are reasons to believe that the changes in TC intensity and size have influenced the storm surge and SSHPI. Table 3 presents our attempt to quantify the contributions of the TC meteorological parameters to the storm surge variations. For this calculation, we individually changed each of the SSHPI parameters, or sets of parameters, to their P2 values, and maintained the other parameters at their P1 averages (Table 2). Changes in TC intensity and size contributed 35% and 32%, respectively, to the overall increase in surge height. Furthermore, their joint contribution may be responsible for as much as 79% of the surge variance. Figure 9 shows similar findings by comparing surge height with the time series diagram of the surge index, which reduces the predictors from the SSHPI into three patterns: (a) V_{max} ; (b) V_{max} and R_{50} ; and (c) V_{max} , R_{50} , and TC translation speed (S). Although surge variance decreases slightly (9%) by the combined influence of wind intensity, size, and translation speed than that of wind intensity and size, the influence of translation speed in storm surge study is not negligible (Rego and Li 2009; Islam and Takagi 2020b; Islam et al. 2021). Nevertheless, it becomes clear from Table 3 and Fig. 9 that changes in TC intensity (V_{max}) may have played the most significant role in the increase of SSHPI and storm surge

magnitudes from 1980 to 2019, followed by changes in TC size (R_{50}). This finding is consistent with the findings of Islam and Takagi (2020a, 2020c), who numerically showed that, at a constant TC wind intensity, the storm surge heights in Tokyo Bay increased linearly as TC size increased, possibly because a large swath of strong winds can affect a larger ocean area for a longer period, inducing larger storm surges. Thus, the observed increases in storm intensity and size shown in Table 2 and Fig. 7 have contributed to the increases in the surge height and SSHPI.

4.2 Changes in TC track

We also inferred the reasons for the increase in storm surge magnitude by analyzing the differences in the TC tracks between P1 and P2. Six-hourly TC best track positions, along with intensity information of landfalling TCs, were analyzed at each grid point from 34° to 37°N and from 137° to 141°E, at 1° intervals (Figs. 10a, 10b). The ratios of the changes in landfalling TC frequency for each grid point (i.e., the ratio of the number of TC central positions in P2 to P1) are shown in Fig. 10c. An overall increase in TC activity is evident in the grids covering the coast of Central Japan. One remarkable feature is a statistically significant increase in TC activity close to Tokyo Bay (near 34°–36°N, 139°–140°E) during P2. In other words, the occurrence frequency of more northeastward TC tracks that impacted Tokyo's shallow coastal areas (Fig. 3b) increased during P2 compared with that during P1 (Fig. 10c and Fig. 2). A significant number of TCs with greater intensities (i.e., $V_{max} \geq 64$ kt)

impacted Tokyo Bay during P2, whereas such TCs occurred at low frequencies during P1 (Fig. 10a, b). Although the storm surge increasing tendency is independent of the TC frequency (discussed in Section 3), changes in the occurrence frequency of more northeastward TC tracks can be regarded as the third most influential factor after V_{max} and R_{50} . Therefore, the large increase in surge magnitude, particularly inside Tokyo Bay (Fig. 6) over the past 40 years, may be attributed to the combined influence of TC intensity, size, and track change.

5. Summary and Conclusions

Based on observational data, the present study demonstrates that storm surge heights in the central coast of Japan, including those in Tokyo, have increased significantly from 1980 to 2019. The SSHPI increased more than three times from P1 to P2, which suggests that the changes in both TC intensity and size at the time of landfall played a significant role in increasing storm surge magnitudes. This finding is consistent with the observation that TCs have become stronger and larger during P2 compared with those during P1. Additionally, the increased occurrence frequency of TCs with more northeastward tracks contributed to the increased surge hazards.

This study suggests that the coast of Central Japan is likely to experience increasing numbers of extreme storm surge events in the future, if the current increasing tendency continues. The coastal flooding of Tokyo and its neighboring cities can affect the Japanese economy substantially because much of the Japanese GDP is concentrated in the Greater

Tokyo area. Thus, our findings are valuable for disaster risk managers, coastal engineers, climate change scientists, and governmental bodies attempting to mitigate the storm surge risk in coastal urban areas. The SSHPI can help explain variations in surge events on regional and local scales, such as the area targeted in this study.

The analyses presented in this study do not constitute the detection or contributions of global warming and climate change impacts on an increasing storm surge tendency. The difference between P1 and P2 could be regarded as a trend associated with global warming, and several recent studies have projected, with high confidence, that sea-level rises that accompany warming will lead to higher storm inundation levels (e.g., Knutson et al. 2019; Knutson et al. 2020; Mori et al. 2021). However, Yamaguchi and Maeda (2020a) reported that this difference may not be distinguishable in the interdecadal variability of such a short period (i.e., 40 years). In addition, significant interdecadal variations exist in TC activity in the WNP basin (i.e., Chan 2016; Li and Zhou 2018). Thus, further research should include quantitative evaluations of the contributions of global warming and interdecadal variations by using numerical simulations.

This study statistically quantifies the contribution of TC meteorological parameters in changing surge hazards. Particularly, we have discussed the possible contribution of TC wind speed, size, and track in changing surge hazards in the coast of Central Japan; nonetheless, other factors such as air pressure and wave set-up can also modulate surge hazards. The physical meaning of these influential factors remains unknown. The present

analyses can be improved further by improving the current data quality, in time and spatial coverage.

Acknowledgments

The first author is thankful to the Ministry of Education, Culture, Sports, Science, and Technology (MEXT) of Japan for the provided scholarship to conduct research in the field of disaster risk reduction. This study was conducted while the first author was participating in the internship at the Atmosphere and Ocean Research Institute, The University of Tokyo. Authors are grateful to Dr. Munehiko Yamaguchi, Japan Meteorological Agency, for providing the approached TC number information for Tokyo area (1980-2019).

Data availability statement

Observed storm tide data can be downloaded from the JMA (<http://www.data.jma.go.jp/kaiyou/db/tide/genbo/index.php>) and JODC (<https://jdoss1.jodc.go.jp/vpage/tide.html>) websites. Predicted tide data can be obtained from the JMA (<http://www.data.jma.go.jp/kaiyou/db/tide/suisan/index.php>) website. TC best track data can be derived from the JMA (<https://www.jma.go.jp/jma/jma-eng/jma-center/rsmc-hp-pub-eg/trackarchives.html>) website.

Disclosure statement

No potential conflict of interest was reported by the author(s).

Funding

This research was funded by the grants awarded to the Tokyo Institute of Technology (Japan

Society for the Promotion of Science, 16KK0121 and 19K04964). This work was also partially supported by a grant awarded to Md. Rezuhanul Islam (The Obayashi Foundation: Overseas Practical Training Grant).

Appendix

Definition and formulation of the SSHPI

The SSHPI is a dimensionless and continuous surge index. It is defined as

$$\text{SSHPI} = \left(\frac{V_{max}}{V_{ref}}\right)^2 \left(\frac{R_{50}}{R_{ref}}\right) \left(\frac{S}{S_{ref}}\right)^a \left(\frac{L_{30}}{L_*}\right), \quad (1)$$

$$\frac{R_{50}}{R_{ref}} = \begin{cases} 1.5 & \text{if } \frac{R_{50}}{R_{ref}} \geq 1.5 \\ \frac{R_{50}}{R_{ref}} & \text{if } 0.5 < \frac{R_{50}}{R_{ref}} < 1.5 \\ 0.5 & \text{if } \frac{R_{50}}{R_{ref}} \leq 0.5 \end{cases}; \quad \left(\frac{S}{S_{ref}}\right)^a = \begin{cases} 1.5 & \text{if } \left(\frac{S}{S_{ref}}\right)^a \geq 1.5 \\ \left(\frac{S}{S_{ref}}\right)^a & \text{if } 0.5 < \left(\frac{S}{S_{ref}}\right)^a < 1.5 \\ 0.5 & \text{if } \left(\frac{S}{S_{ref}}\right)^a \leq 0.5 \end{cases}$$

where, V_{max} is the maximum sustained TC wind speed (kt), R_{50} is a measure of the radius of the 50 kt (26 m s^{-1}) winds (arithmetic average of the longest and shortest R_{50} , in nautical miles (NM)), S is the translation speed (km h^{-1}), a is the characteristic coastal geometry (for open coasts, $a = 1$ and for semi-enclosed bays, $a = -1$), and L_{30} is the horizontal distance (km) between the shoreline and the 30 m depth contour. A GIS environment (ArcMap 10.3) was used to measure the closest horizontal distance between each selected tide station and the 30 m depth contour (i.e., Fig. 3b). V_{ref} , R_{ref} , and S_{ref} , are reference constants, as follows: 50 kt equivalents of the tropical storm category, 95 NM (historical mean R_{50} at the time of landfall in Japan), and 35 km h^{-1} (historical mean S at the time of landfall in Japan), respectively (Islam et al. 2021). L_* was chosen to be 30 km to make the SSHPI roughly equal

in magnitude to the peak storm surge heights observed in the study area.

The mathematical equation for the SSHPI (eq. 1) adopts and modifies those previous surge indexes, specifically, the hurricane surge index (HSI; eq. 2; Kantha 2006, 2008) and surge scale (SS; eq. 3; Irish and Resio 2010), and further adds a coastal geometry parameter (a) and TC forward speed information (S) (Islam and Takagi 200b).

$$HSI = \left(\frac{V_{max}}{V_{ref}}\right)^2 \left(\frac{R_{33}}{R_{ref}}\right), \quad (2)$$

$$SS = (2.43E - 4) \Delta p L_{30m} \Psi_x \left(\frac{R_{33}}{L_{30m}}\right), \quad (3)$$

$$\Psi_x \left(\frac{R_{33}}{L_{30m}}\right) = \left(\frac{R_{33}}{L_{30m}}\right) \text{ when } \left(\frac{R_{33}}{L_{30m}}\right) \leq 1 \text{ and } \Psi_x \left(\frac{R_{33}}{L_{30m}}\right) = 1 \text{ when } \left(\frac{R_{33}}{L_{30m}}\right) > 1$$

R_{33} is the radius of hurricane force wind (64 kt), Δp is the TC central pressure difference, which is defined as the nominal atmospheric pressure around a TC minus the central pressure of that TC and is directly proportional to the V_{max}^2 . In eq. 3, $\left(\frac{R_{33}}{L_{30m}}\right)$ is the ratio of the storm size to L_{30m} and Ψ_x is the dimensionless storm size function to adjust that ratio. V_{ref} and R_{ref} in eq. 2 are the climatological reference constants: 33 m/s and 96.6 km.

The SSHPI (eq. 1) and HSI (eq. 2) have quadratic dependence to V_{max} because wind momentum input at the water surface is proportional to V_{max}^2 . The reason for the linear dependence of surge indexes on the storm radius is because the storm surge impact is most often confined to a broad but roughly linear strip along the coastline (Kantha 2008). Another underlying assumption is that integration of storm size and wind strength over the footprint of the TC provides a bulk amount of energy/momentum transferred from the storm to the

water column, and thus, the total water level functionally depends on the velocity and storm radius (Islam et al. 2021). Furthermore, the relationship between R_{50} and storm surge forecasting has been discussed in many prior studies (e.g., Takagi and Wu 2016; Klotzbach et al. 2020; Islam and Takagi 2020a). The linear dependence of the SSHPI on TC forward speed is twofold. First, in semi-enclosed bays, the effective cross-shore shallow area over which TC winds act is larger and the time scale for mass redistribution (to generate a sea surface slope) is on the order of hours, which is longer than along the open coasts. Thereby, with cross-shore wind stress components, a slower TC has more time to interact with the seawater and pushes more into shallow areas of a bay (Mastenbroek et al. 1993; Weisberg and Zheng 2006; Islam and Takagi 2020a, 2020b). On the contrary, in the open coastlines, it is plausible that a fast-moving TC would energize a shelf wave and cause an increased storm surge because the TC translation speed tends to coincide with the long-wave propagation speed (Proudman 1953; Rego and Li 2009). L_{30m} is used in eq. 1 and eq. 3 because Irish and Resio (2010) and Chavas et al. (2013) has reported that L_{30m} is an optimal characteristic length scale for storm surge generation in the US coasts.

A stationary or very slow-moving TC (i.e., $S = 5$ km/h) would result in very low SSHPI numbers (using eq. 1) on the open coast and extremely high numbers in semi-enclosed bays (and vice-versa). TC with a very large size (i.e., $R_{50} = 170$ nm) would also result in very high SSHPI numbers (and vice-versa). However, such TCs are infrequent in Japan, but can sometimes occur elsewhere. Compared to V_{max} and L_{30m} , the upper and lower bound of TC

size ($0.5 \leq \frac{R_{50}}{R_{ref}} \leq 1.5$) and forward speed ($0.5 \leq (\frac{S}{S_{ref}})^a \leq 1.5$) in eq. 1 restricts their contribution in generating surge hazards and, thus, prevents discrete jumps in the SSHPI. In this study, the reference constants (V_{ref} , R_{ref} , and S_{ref}) represent a baseline TC event that occurs relatively frequently. This suggests that large (i.e., $R_{50} > 95$ nm) and quickly moving (i.e., $S > 35$ km h⁻¹) intense (i.e., $V_{max} > 50$ kt) TCs will generate a larger storm surge along open coasts, whereas bays are more susceptible to large, slowly moving (i.e., $S < 35$ km h⁻¹) intense TCs.

Furthermore, the SSHPI does not directly consider the inverse barometer effect (IBE) and the influence of the TC approach angle, waves, and astronomical tide, to keep the SSHPI simple. Thus, the SSHPI will tend to underestimate/overestimate total surge height somewhat for some TC events. The limitation is particularly relevant in open coasts, where wave set-up and IBE are often the dominant drivers behind storm surge and coastal flooding. SSHPI was derived to explain distinctive surge characteristics between open coasts and bays. On the other hand, the prediction with SSHPI was not fully verified for locations in middle point of a bay and open coast. Furthermore, a very steep coast (i.e., $L_{30m} = 0.5$ km) would result in a low SSHPI number (using eq. 1); however, a strong TC could still cause significant storm surge (Islam et al. 2021). Lastly, the SSHPI is largely dependent on the quality of the input parameters. The correlation statistics for the SSHPI shown in this study will improve as the uncertainties (Landsea and Franklin 2013) associated with the TC information become smaller.

References

- Anh, L. T., H. Takagi, M. Heidarzadeh, Y. Takata, and A. Takahashi, 2019: Field Surveys and Numerical Simulation of the 2018 Typhoon Jebi: Impact of High Waves and Storm Surge in Semi-enclosed Osaka Bay, Japan, *Pure Appl Geophys*, **176**(10), 4139–4160. <https://doi.org/10.1007/s00024-019-02295-0>
- Blake, E. S., T. B. Kimberlain, R. J. Berg, J. P. Cangialosi, and J. L. Beven, 2013: *Tropical cyclone report Hurricane Sandy (AL182012) 22 – 29 October 2012*. National Weather Service, National Hurricane Center, October 2012, 1–157.
- Bromirski, P. D., R. E. Flick, and D. R. Cayan, 2003: Storminess Variability along the California Coast: 1858-2000. *J. Clim.*, **16**(6), 982–993. [https://doi.org/10.1175/1520-0442\(2003\)016<0982:SVATCC>2.0.CO;2](https://doi.org/10.1175/1520-0442(2003)016<0982:SVATCC>2.0.CO;2)
- Brown, S., R. J. Nicholls, C. D. Woodroffe, S. Hanson, J. Hinkel, A. S. Kebede, B. Neumann, and A. T. Vafeidis, 2013: Sea-level rise impacts and responses: A global perspective. *Coastal hazards*. Finkl, W. (ed.), Springer, 117–149. https://doi.org/10.1007/978-94-007-5234-4_5
- Chan, J. C. L., 2016: Observed Variations of Western North Pacific Tropical Cyclone Activity on Decadal Time Scales and Longer. *Climate Change: Multidecadal and Beyond*. Chang, C.-P., M. Ghil, M. Latif, and J. M. Wallace (eds.), World Scientific Publishing, 303-313. https://doi.org/10.1142/9789814579933_0019
- Chan, K. T. F., 2019: Are global tropical cyclones moving slower in a warming climate?

Environ. Res. Lett., **14**(10). 104015. <https://doi.org/10.1088/1748-9326/ab4031>

Chavas, D., E. Yonekura, C. Karamperidou, N. Cavanaugh, and K. Serafin, 2013: U.S. Hurricanes and Economic Damage: Extreme Value Perspective. *Nat Hazards Rev.*, **14**(4), 237–246. [https://doi.org/10.1061/\(ASCE\)NH.1527-6996.0000102](https://doi.org/10.1061/(ASCE)NH.1527-6996.0000102)

Church, J. A., J. R. Hunter, K. L. McInnes, and N. J. White, 2006: Sea-level rise around the Australian coastline and the changing frequency of extreme sea-level events. *Aust. Meteorol. Mag.*, **55**, 253–260.

Elsner, J., and K. Liu, 2003: Examining the ENSO-typhoon hypothesis. *Clim. Res.*, **25**(1), 43–54. <https://doi.org/10.3354/cr025043>

Esteban, M., H. Takagi, and T. Shibayama, 2015: Introduction: Lessons from the Last 10 Years of Coastal Disasters. *Handbook of Coastal Disaster Mitigation for Engineers and Planners*. Esteban, M., H. Takagi, and T. Shibayama (Eds.), Elsevier, xxv–xxx. <https://doi.org/10.1016/B978-0-12-801060-0.09996-2>

Hallegatte, S., C. Green, R. J. Nicholls, and J. Corfee-Morlot, 2013: Future flood losses in major coastal cities. *Nat. Clim. Chang.*, **3**(9), 802–806. <https://doi.org/10.1038/nclimate1979>

Huang X., X. Peng, J. Fei, X. Cheng, J. Ding, and D. Yu, 2021. Evaluation and error analysis of official tropical cyclone intensity forecasts during 2005–2018 for the western North Pacific. *J. M. Soc. Japan* **99**(1), 139–163. <https://doi.org/10.2151/jmsj.2021-008>

Irish, J. L., D. T. Resio, and J. J. Ratcliff, 2008: The influence of storm size on hurricane

- surge. *J. Phys. Oceanogr.*, **38**(9), 2003–2013. <https://doi.org/10.1175/2008JPO3727.1>
- Irish, J. L., and D. T. Resio, 2010: A hydrodynamics-based surge scale for hurricanes. *Ocean Eng.*, **37**(1), 69–81. <https://doi.org/10.1016/j.oceaneng.2009.07.012>
- Islam, M. R., C-Y. Lee, K. T. Mandli, and H. Takagi, 2021: A new tropical cyclone surge index incorporating the effects of coastal geometry, bathymetry and storm information. *Sci. Rep.*, **11**(1). <https://doi.org/10.1038/s41598-021-95825-7>
- Islam, M. R., and H. Takagi, 2020a: Typhoon parameter sensitivity of storm surge in the semi-enclosed Tokyo Bay. *Front. Earth. Sci.*, **14**(3), 553–567. <https://doi.org/10.1007/s11707-020-0817-1>
- Islam, M. R., and H. Takagi, 2020b: Statistical significance of tropical cyclone forward speed on storm surge generation: retrospective analysis of best track and tidal data in Japan. *Georisk*. <https://doi.org/10.1080/17499518.2020.1756345>
- Islam, M. R., and H. Takagi, 2020c: On the Importance of Typhoon Size in Storm Surge Forecasting. *Water, Flood Management and Water Security Under a Changing Climate*, Haque, A., and A. Chowdhury (eds.), Springer, 153–162. https://doi.org/10.1007/978-3-030-47786-8_10
- Islam, M. R., H. Takagi, L. T. Anh, A. Takahashi, and K. Bowei, 2018: 2017 Typhoon Lan reconnaissance field survey in coasts of Kanto region, Japan. *J. Japan Soc. Civ. Eng. Ser. B3 (Ocean Eng.)*, **74**(2), 593-598. https://doi.org/10.2208/jscejoe.74.i_593
- Japan Meteorological Agency, 2020a: Best Track Data. <https://www.jma.go.jp/jma/jma->

eng/jma-center/rsmc-hp-pub-eg/trackarchives.html (Accessed on December 20, 2020)

Japan Meteorological Agency, 2020b: Forecast terms related to typhoons.

http://www.jma.go.jp/jma/kishou/known/yougo_hp/haichi2.html (Accessed on December 20, 2020)

Japan Meteorological Agency, 2020c: Tide Stations.

<https://doi.org/10.7551/mitpress/10659.003.0018> (Accessed on December 20, 2020)

Japan Meteorological Agency, 2020d: Predicted Tide Stations.

<http://www.data.jma.go.jp/kaiyou/db/tide/suisan/index.php> (Accessed on December 20, 2020)

JMA. Japan Meteorological Agency, 2019: Outline NWP 2019.

<https://www.jma.go.jp/jma/jma-eng/jma-center/nwp/outline2019-nwp/index.htm>
(Accessed on December 20, 2020)

Japan Aerospace Exploration Agency, 2015: ALOS World 3D - 30m.

<https://www.eorc.jaxa.jp/ALOS/en/aw3d30/index.html> (Accessed on December 20, 2020)

Japan Oceanographic Data Center, 2020a: 500m Gridded Bathymetry Data.

<https://www.jodc.go.jp/jodcweb/JDOSS/infoJEGG.html> (Accessed on December 20, 2020)

Japan Oceanographic Data Center, 2020b: Tide Stations.

<https://jdoss1.jodc.go.jp/vpage/tide.html> (Accessed on December 20, 2020)

- Kantha, L., 2006: Time to replace the Saffir-Simpson hurricane scale? *Eos*, **87**(1), 3–6.
<https://doi.org/10.1029/2006EO010003>
- Kantha, L., 2008: Comments on "Tropical cyclone destructive potential by integrated kinetic energy. *Bull. Amer. Meteor. Soc.*, **89**(2), 219–221.
- Kato, F. and K. Torii, 2004: Risk assessment on storm surge floods. *Asian and Pacific Coasts 2003*, 1–13. https://doi.org/10.1142/9789812703040_0133
- Klotzbach, P. J., M. M. Bell, S. G. Bowen, E. J. Gibney, K. R. Knapp and C. J. Schreck III, 2020: Surface Pressure a More Skillful Predictor of Normalized Hurricane Damage than Maximum Sustained Wind. *Bull. Amer. Meteor. Soc.*, **101**, E830–E846.
<https://doi.org/10.1175/BAMS-D-19-0062.1>
- Knutson, T., S. J. Camargo, J. C. L. Chan, K. Emanuel, C. H. Ho, J. Kossin, M. Mohapatra, M. Satoh, M. Sugi, K. Walsh, and L. Wu, 2019: Tropical cyclones and climate change assessment. *Bull. Am. Meteorol. Soc.*, **100**(10), 1987–2007.
<https://doi.org/10.1175/BAMS-D-18-0189.1>
- Knutson, T., S. J. Camargo, J. C. L. Chan, K. Emanuel, C. H. Ho, J. Kossin, M. Mohapatra, M. Satoh, M. Sugi, K. Walsh, and L. Wu, 2020: Tropical cyclones and climate change assessment part II: Projected response to anthropogenic warming. *Bull. Am. Meteorol. Soc.*, **101**(3), E303–E322. <https://doi.org/10.1175/BAMS-D-18-0194.1>
- Landsea, C. W. and J. L. Franklin, 2013: Atlantic Hurricane Database Uncertainty and Presentation of a New Database Format. *Mon. Weather Rev.*, **141**, 3576–3592.

<https://doi.org/10.1175/MWR-D-12-00254.1>

LI, R. C. Y., and W. ZHOU, 2018: Revisiting the intraseasonal, interannual and interdecadal variability of tropical cyclones in the western North Pacific. *Atmos. Ocean. Sci. Lett.*, **11**(2), 198–208. <https://doi.org/10.1080/16742834.2018.1459460>

Mastenbroek, C., G. Burgers and P. A. E. M. Janssen, 1993: The Dynamical Coupling of a Wave Model and a Storm Surge Model through the Atmospheric Boundary Layer. *J. Phys. Oceanogr.* **23**, 1856–1866. [https://doi.org/10.1175/1520-0485\(1993\)023<1856:TDCOAW>2.0.CO;2](https://doi.org/10.1175/1520-0485(1993)023<1856:TDCOAW>2.0.CO;2)

Moon, I. J., S. H. Kim, and J. C. L. Chan, 2019: Climate change and tropical cyclone trend. *Nature*, **570**(7759), E3–E5. <https://doi.org/10.1038/s41586-019-1222-3>

Mori, N., N. Ariyoshi, T. Shimura, T. Miyashita, and J. Ninomiya, 2021: Future projection of maximum potential storm surge height at three major bays in Japan using the maximum potential intensity of a tropical cyclone. *Clim. Chang* (accepted).

Menéndez, M., and P. L. Woodworth, 2010: Changes in extreme high water levels based on a quasi-global tide-gauge data set. *J. Geophys. Res.*, **115**(C10), C10011. <https://doi.org/10.1029/2009JC005997>

Neumann, B., A. T. Vafeidis, J. Zimmermann, and R. J. Nicholls, 2015: Future coastal population growth and exposure to sea-level rise and coastal flooding - A global assessment. *PLoS ONE*, **10**(3). <https://doi.org/10.1371/journal.pone.0118571>

Nicholls, R. J., and A. Cazenave, 2010: Sea-level rise and its impact on coastal zones.

Science, **328**(5885), 1517–1520. <https://doi.org/10.1126/science.1185782>

Omori, F 1918: *Tsunami in Tokyo Bay*. In: Earthquake Investigation Committee Report, 89, 19 – 48 (in Japanese).

Proudman, J, 1953: *Dynamical Oceanography*. Wiley.

Rego, J. L. and C. Li, 2009: On the importance of the forward speed of hurricanes in storm surge forecasting: A numerical study. *Geophys. Res. Lett.*, **36**, L07609. <https://doi.org/10.1029/2008GL036953>

Sebastian, A., J. Proft, J. C. Dietrich, W. Du, P. B. Bedient, and C. N. Dawson, 2014: Characterizing hurricane storm surge behavior in Galveston Bay using the SWAN+ADCIRC model. *Coast. Eng.*, **88**, 171–181. <https://doi.org/10.1016/j.coastaleng.2014.03.002>

Shimozono, T., Y. Tajima, K. Kumagai, T. Arikawa, Y. Oda, Y. Shigihara, N. Mori, and T. Suzuki, 2020: Coastal impacts of super typhoon Hagibis on Greater Tokyo and Shizuoka areas, Japan. *Coast. Eng. J.*, **62**(2), 129–145. <https://doi.org/10.1080/21664250.2020.1744212>

Swiss Re, 2013: *Mind the risk A global ranking of cities under threat from natural disasters*. Swiss Re. <http://repo.floodalliance.net/jspui/handle/44111/1600>

Takagi, H. and W. Wu, 2016: Maximum wind radius estimated by the 50 kt radius: improvement of storm surge forecasting over the western North Pacific. *Nat. Hazards Earth Syst. Sci.*, **16**, 705–717. <https://doi.org/10.5194/nhess-16-705-2016>

- Takagi, H., M. R. Islam, L. T. Anh, A. Takahashi, T. Sugiu, and F. Furukawa, 2020: Investigation of high wave damage caused by 2019 Typhoon Faxai in kanto region and wave hindcast in Tokyo Bay. *J. Japan Soc. Civ. Eng. Ser. B3 (Ocean Eng.)*, **76**(1), 12–21. https://doi.org/10.2208/jscejoe.76.1_12
- Takagi, H., Takahashi, A., 2021: Short-fetch high waves during the passage of 2019 Typhoon Faxai over Tokyo Bay. *Front. Earth. Sci.*, **15**(2). <https://doi.org/10.1007/s11707-021-0872-2>
- United Nations Population Division, 2018: *The World 's Cities in 2018. United Nation.*
- Weisberg, R. H. and L. Zheng, 2006: Hurricane storm surge simulations for Tampa Bay. *Estuaries Coast*, **29**, 899–913. <https://doi.org/10.1007/BF02798649>
- Woodworth, P. L., and D. L. Blackman, 2004: Evidence for systematic changes in extreme high waters since the mid-1970s. *J. Clim*, **17**(6), 1190–1197. [https://doi.org/10.1175/1520-0442\(2004\)017<1190:EFSCIE>2.0.CO;2](https://doi.org/10.1175/1520-0442(2004)017<1190:EFSCIE>2.0.CO;2)
- Yamaguchi, M., and S. Maeda, 2020a: Increase in the number of tropical cyclones approaching tokyo since 1980. *J. Meteorol. Soc. Japan*, **98**(4), 775–786. <https://doi.org/10.2151/jmsj.2020-039>
- Yamaguchi, M., and S. Maeda, 2020b: Slowdown of Typhoon Translation Speeds in Mid-latitudes in September Influenced by the Pacific Decadal Oscillation and Global Warming. *J. Meteorol. Soc. Japan, Ser. II*, **98**(6), 1321–1334. <https://doi.org/10.2151/jmsj.2020-068>

List of Figures

Fig. 1 All TCs that made landfall (as per the criteria considered for the selection of TC) around Japan Central Coast (34° – 36° N, 137° – 141° E) in 1980-2019 (JMA, 2020a). The black-colored box indicates the area of interest.

Fig. 2 TC landfall points (as per the criteria considered for the selection of TC) along the Japan Central Coast in 1980-2019.

Fig. 3 Location map of tide observation stations (a) Maisaka, Omaezaki, Shimizuminato, Uchiura, and Irouzaki; (b) Yokohama, Tokyo, Chiba, Mera, and Choshi (JODC, 2000a; JAXA, 2015; JMA, 2020a). TC tracks represent TCs affected the study area in 1980-2019 (as per the criteria considered for the selection of TC).

Fig. 4 Time series of (a) annual mean storm surge height (cm); (b) annual peak storm surge height (cm) along the Japan Central Coast over 40 years from 1980-2019. Gray shading indicates the two-sided 95% confidence bounds around the linear regression line. The difference in the storm surge height averaged over 1980-1999 and 2000-2019 is statistically significant at the 95% level.

Fig. 5 Change in the annual mean storm surge distribution along the coast of central Japan. The changes are shown between P1 (1980-1999) and P2 (2000-2019). Error bars show two-sided 95% confidence intervals.

Fig. 6 Spatial distribution of storm surge change statistics between P1 (1980-1999) and P2 (2000-2019) along the coast of Central Japan.

Fig. 7 Average annual number of landfalling TC (as per the criteria considered for the selection of TC) along the coast of Central Japan in 1980-2019 as a function of the (a) maximum sustained wind speed (kt); (b) radius of 50-kt wind (NM); (c) translation speed (km h⁻¹) at the landfall time frame.

Fig. 8 A measure of the storm surge hazard potential by tropical cyclones affected Japan Central Coast compared to annual mean storm surge height in 1980-2019.

Fig. 9 Comparison between annual mean storm surge heights observed along the Japan Central Coast during 1980-2019 and possible contribution of TC meteorological parameters in SSHPI. See also Table 3.

Fig. 10 Landfalling TC six-hourly best track position along with intensity information bounded

in latitude by 34°N and 37°N , and longitude by 137°E and 141°E . in (a) 1980-1999; (b) 2000-2019; (c) The change in the landfalling TC activity (the number of TCs central position in 2000-2019 divided by that in 1980-1999; green colored number) in each grid.

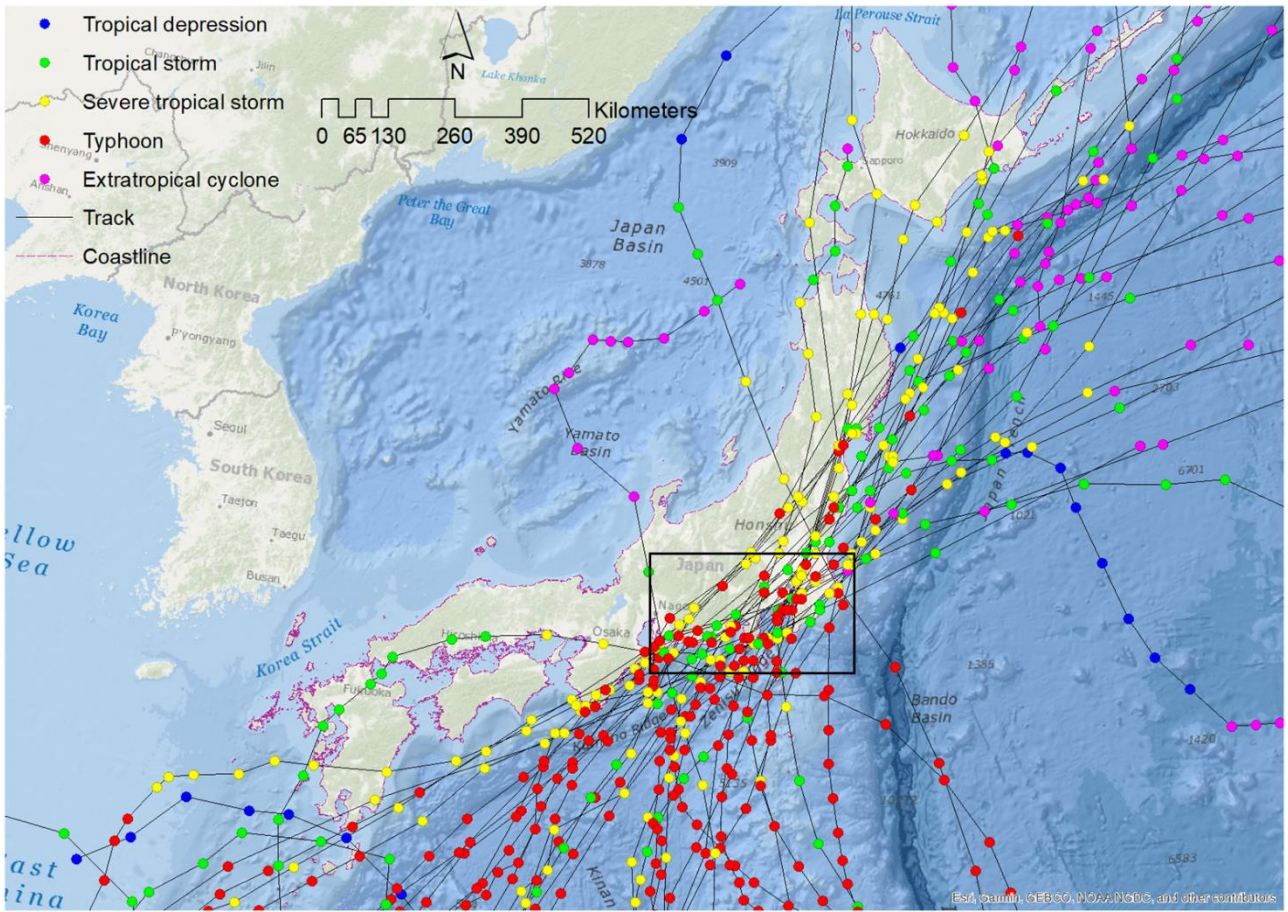


Fig. 1 All TCs that made landfall (as per the criteria considered for the selection of TC) around Japan Central Coast (34° – 36° N, 137° – 141° E) in 1980-2019 (JMA, 2020a). The black-colored box indicates the area of interest.

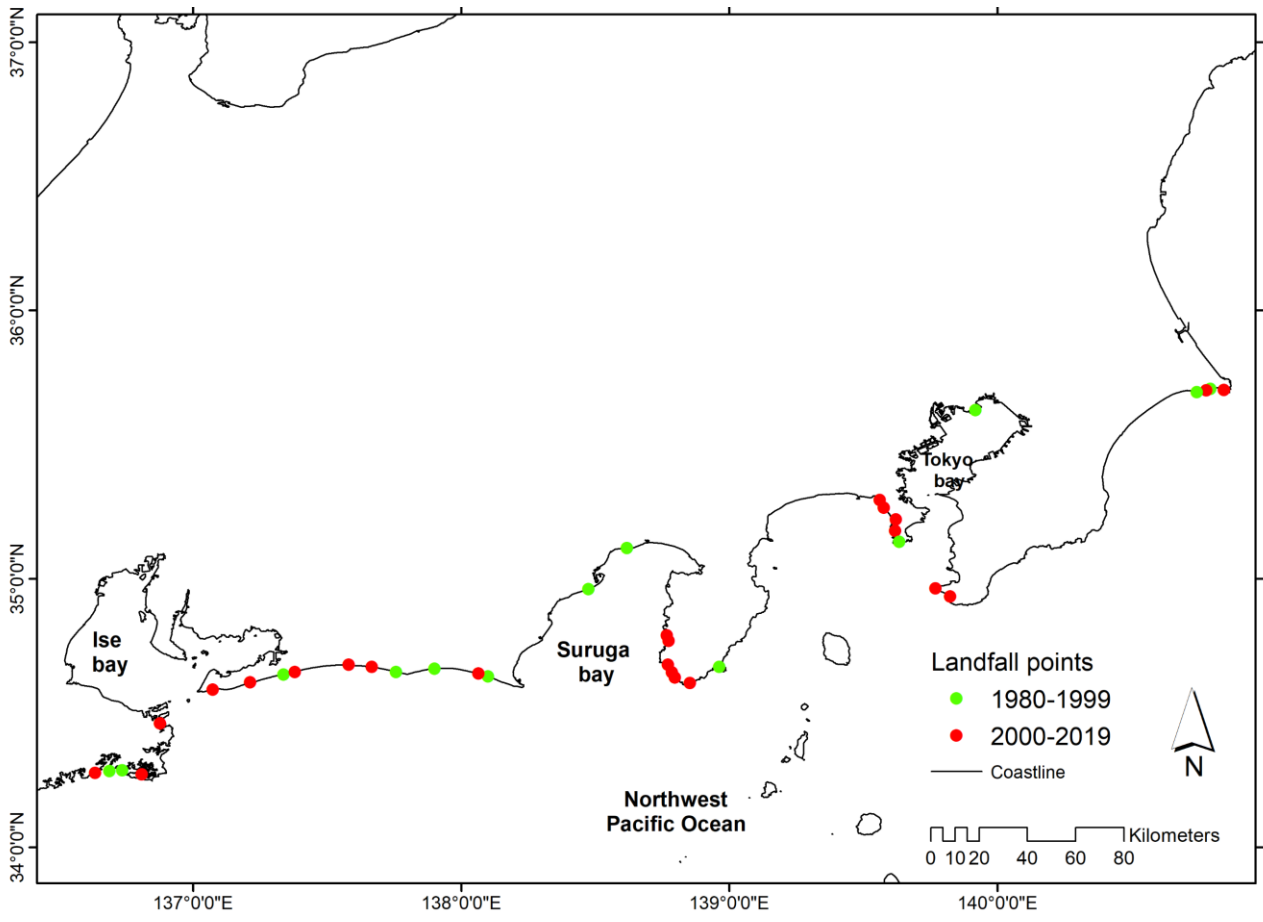


Fig. 2 TC landfall points (as per the criteria considered for the selection of TC) along the Japan Central Coast in 1980-2019.

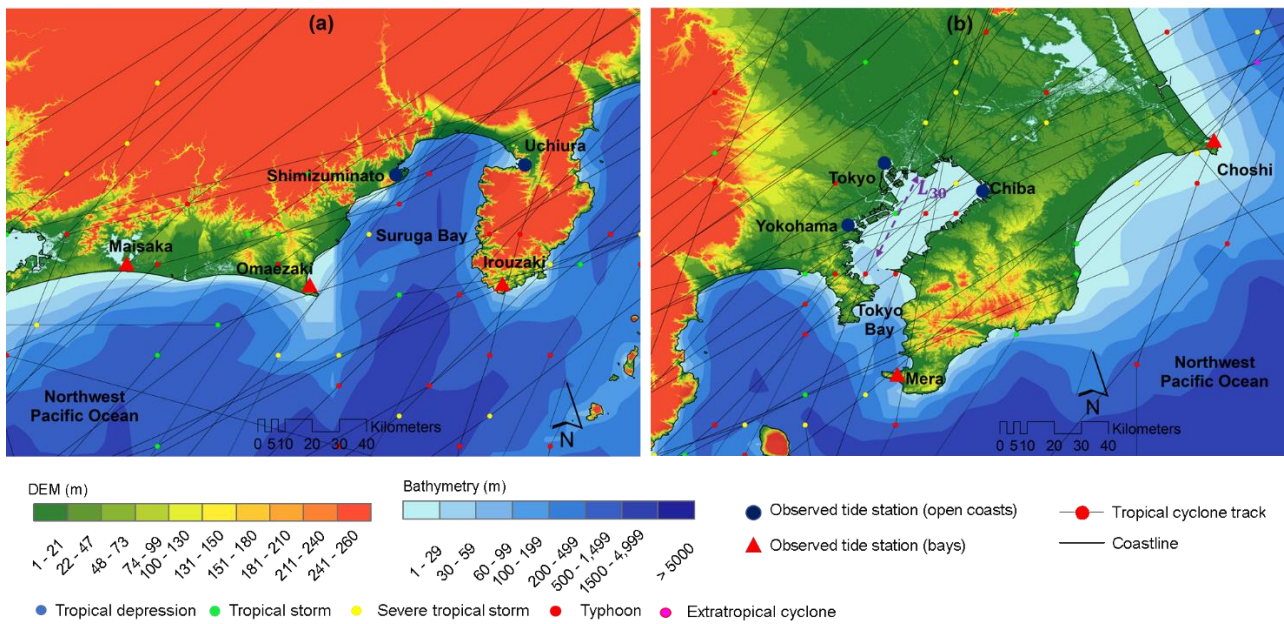
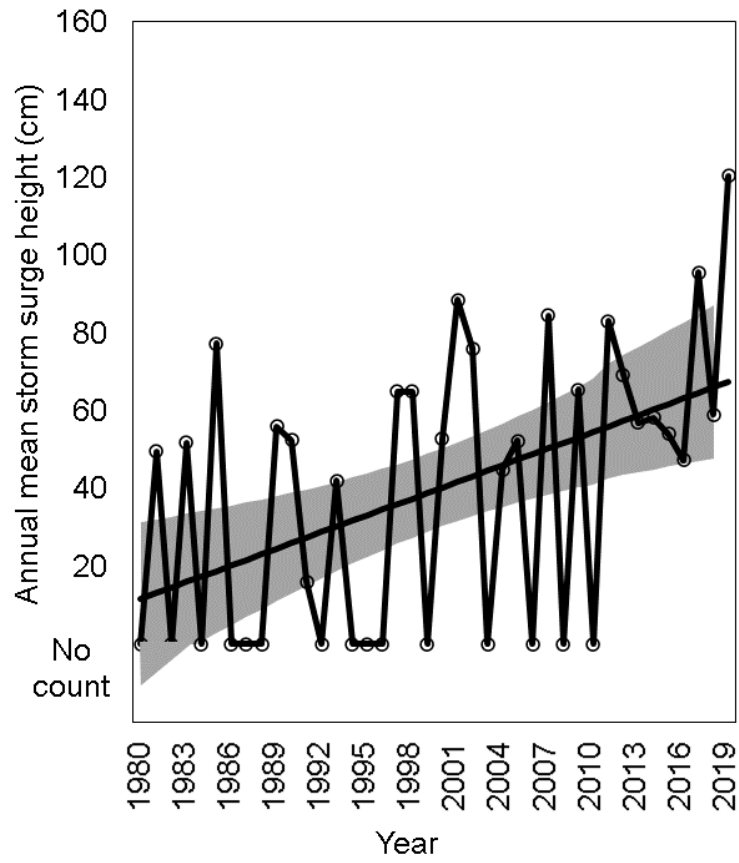


Fig. 3 Location map of tide observation stations (a) Maisaka, Omaezaki, Shimizuminato, Uchiura, and Irouzaki; (b) Yokohama, Tokyo, Chiba, Mera, and Choshi (JODC, 2000a; Japan Aerospace Exploration Agency, 2015; JMA, 2020a). TC tracks represent TCs affected the study area in 1980-2019 (as per the criteria considered for the selection of TC).

(a)



(b)

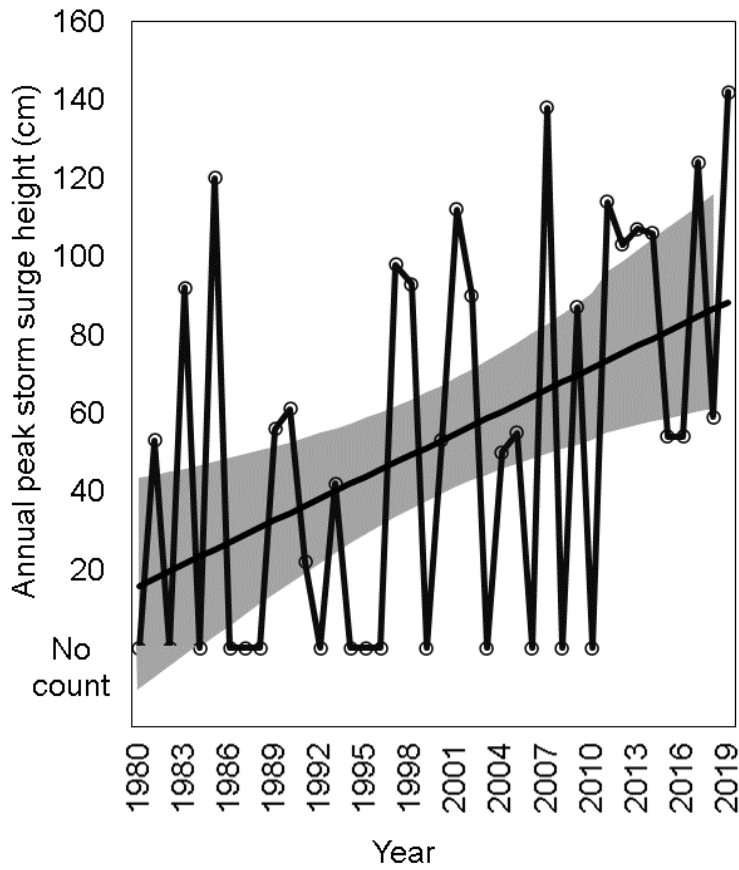


Fig. 4 Time series of (a) annual mean storm surge height (cm); (b) annual peak storm surge height (cm) along the Japan central coast over 40 years from 1980-2019. Gray shading indicates the two-sided 95% confidence bounds around the linear regression line. The difference in the storm surge height averaged over 1980-1999 and 2000-2019 is statistically significant at the 95% level.

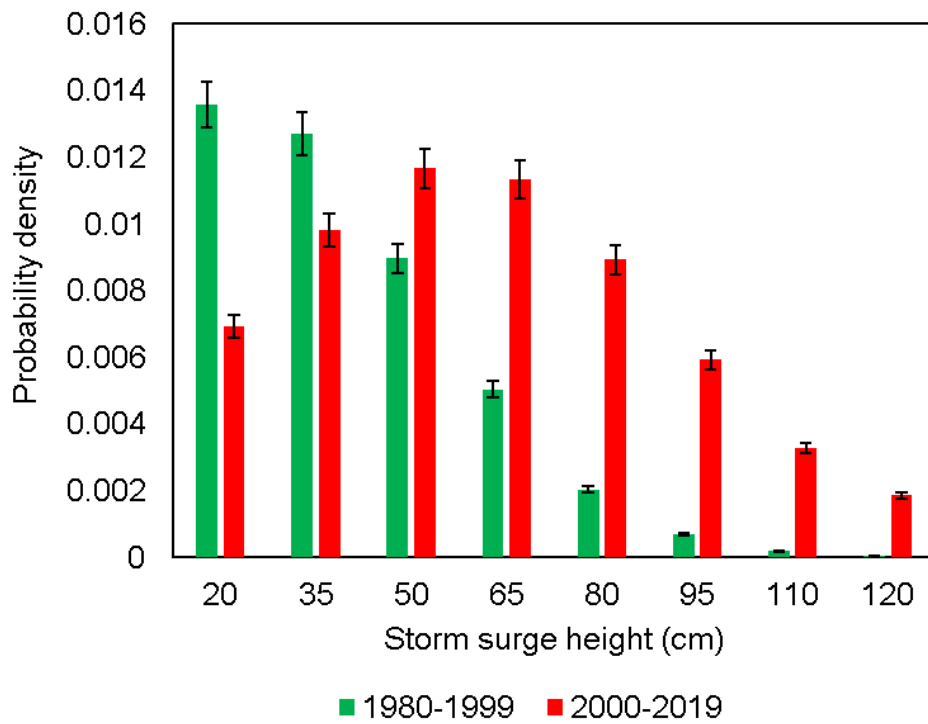


Fig. 5 Change in the annual mean storm surge distribution along the coast of Central Japan. The changes are shown between P1 (1980-1999) and P2 (2000-2019). Error bars show two-sided 95% confidence intervals.

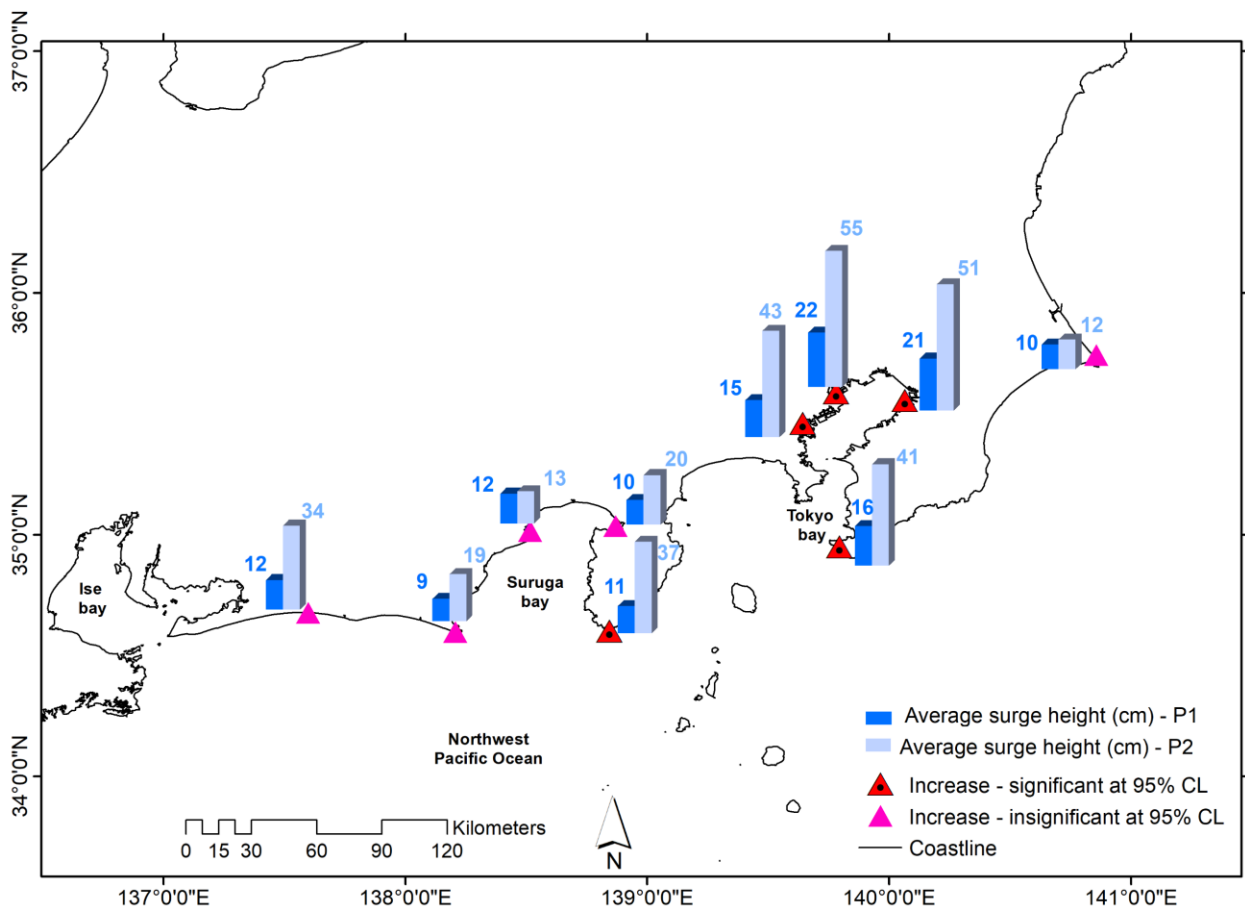


Fig. 6 Spatial distribution of storm surge change statistics between P1 (1980-1999) and P2 (2000-2019) along the coast of Central Japan.

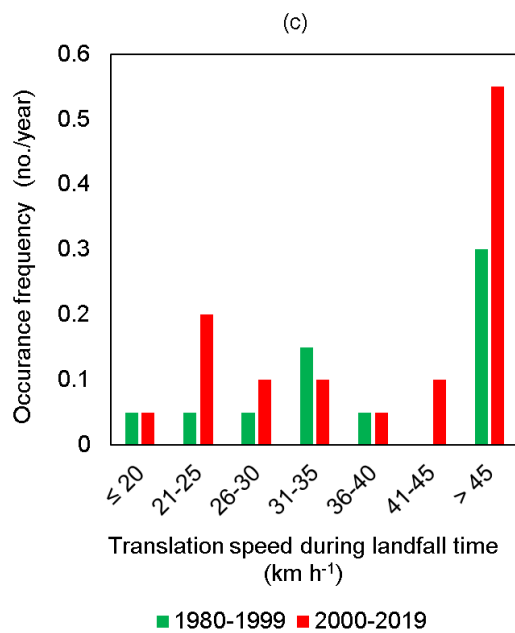
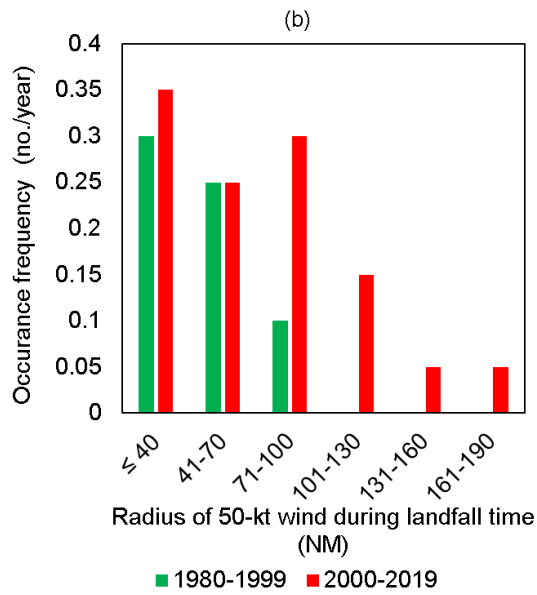
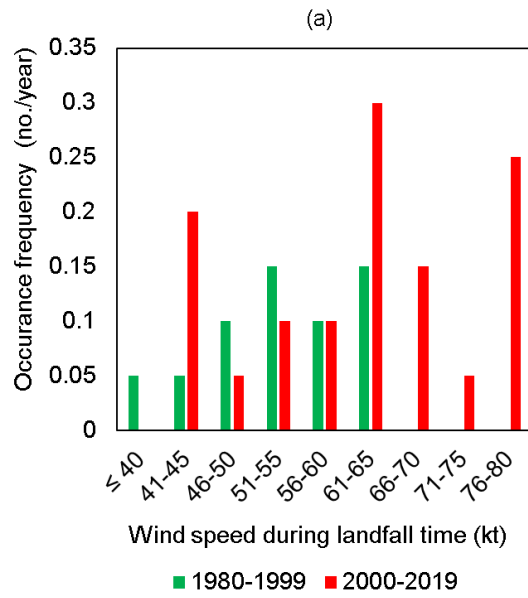


Fig. 7 Average annual number of landfalling TC (as per the criteria considered for the selection of TC) along the coast of Central Japan in 1980-2019 as a function of the (a) maximum sustained wind speed (kt); (b) radius of 50-kt wind (NM); (c) translation speed (km h⁻¹) at the landfall time frame.

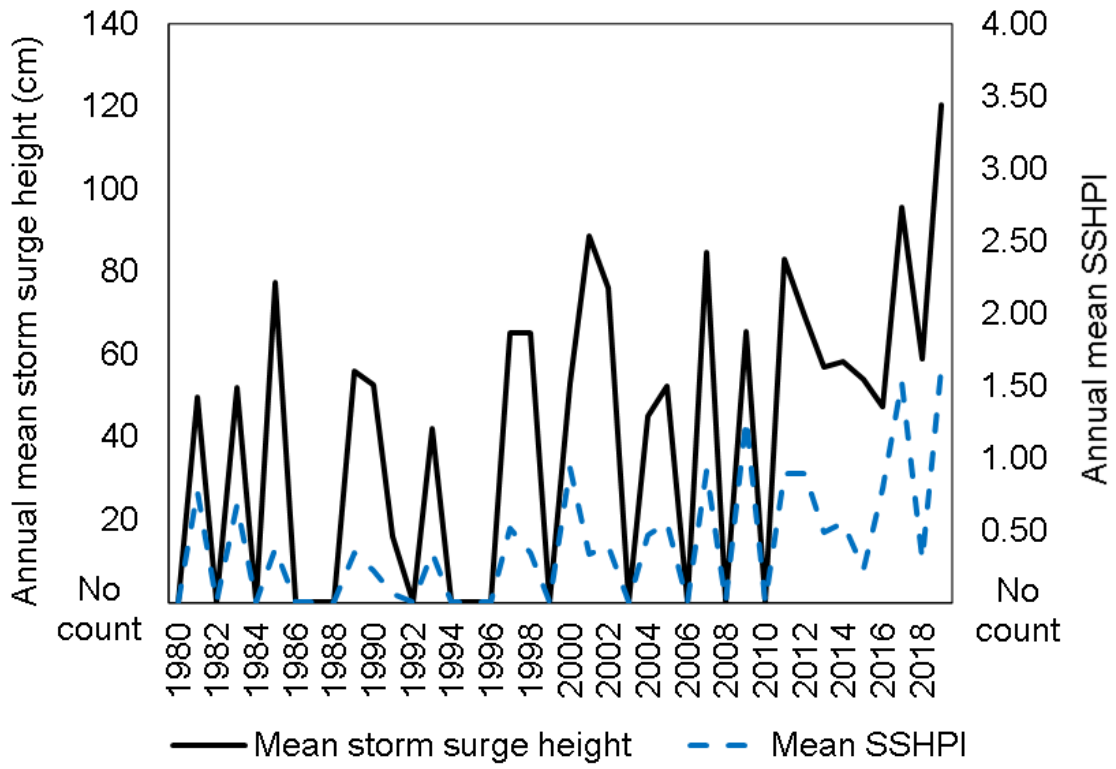


Fig. 8 A measure of the storm surge hazard potential by tropical cyclones affected Japan Central Coast compared to annual mean storm surge height in 1980-2019.

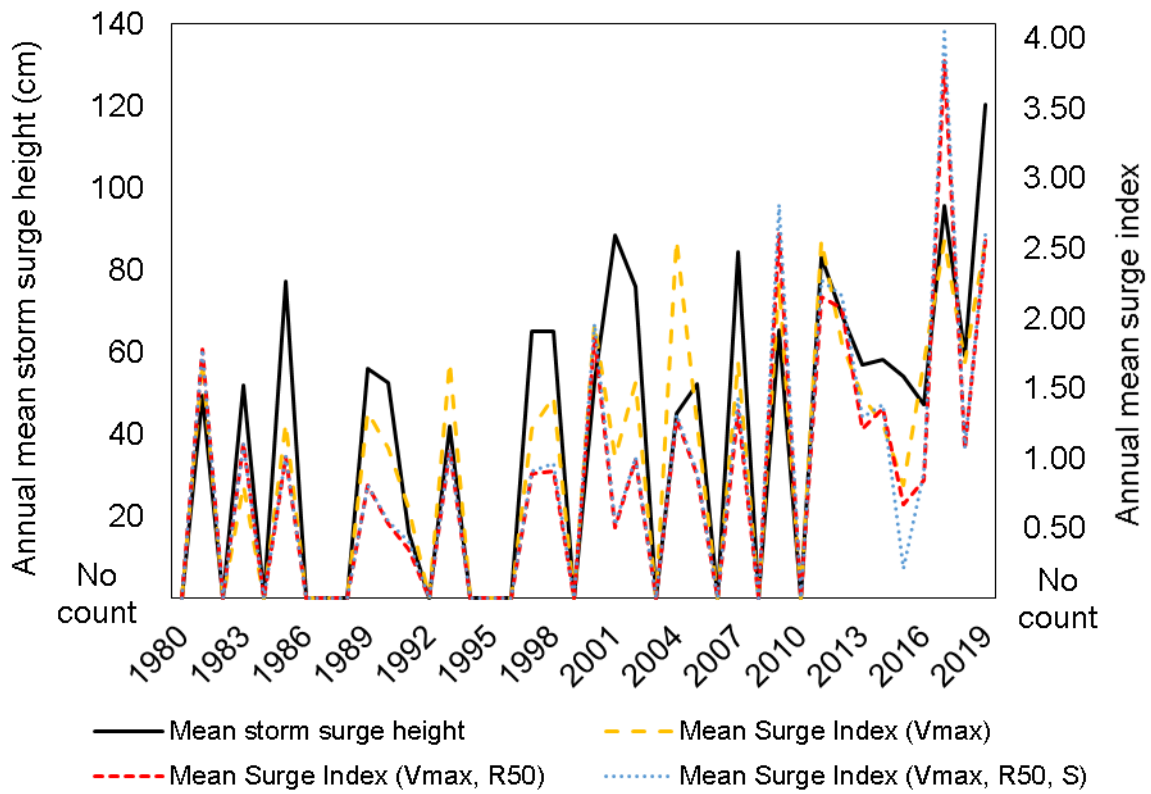
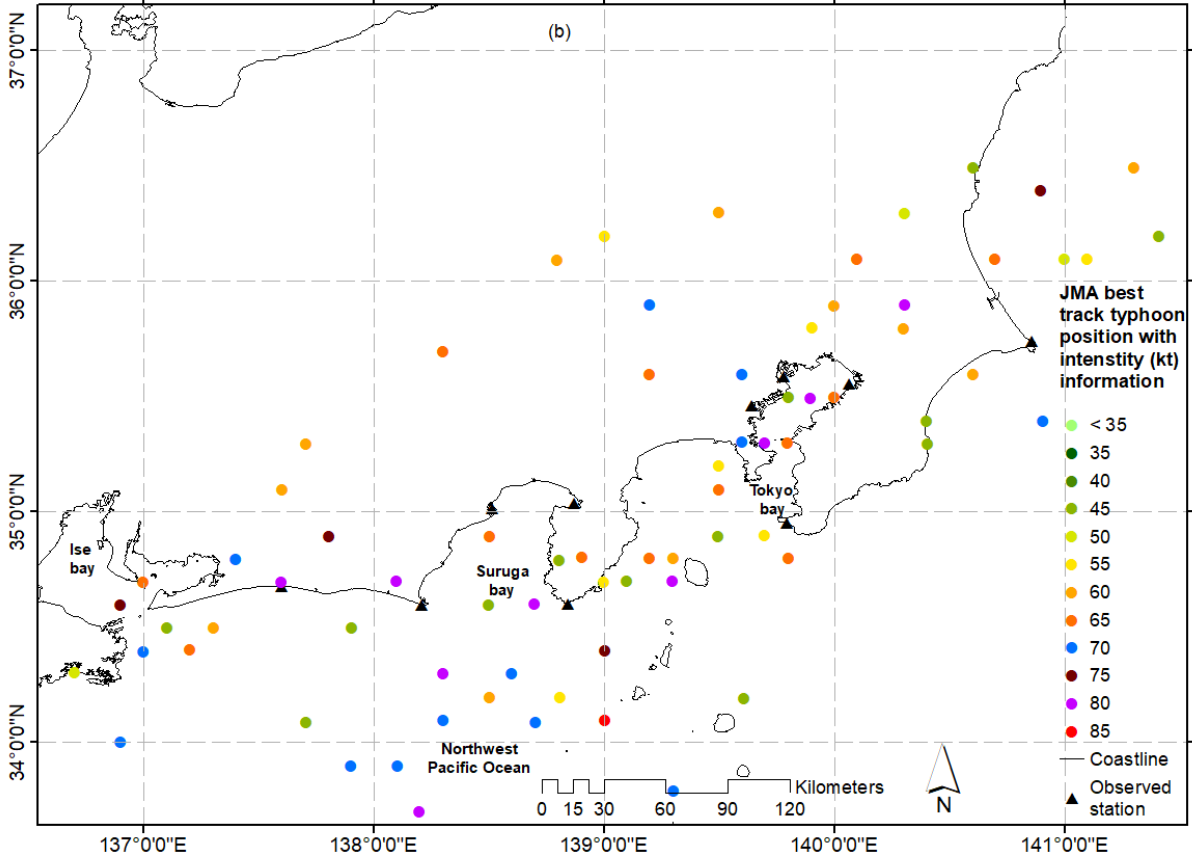
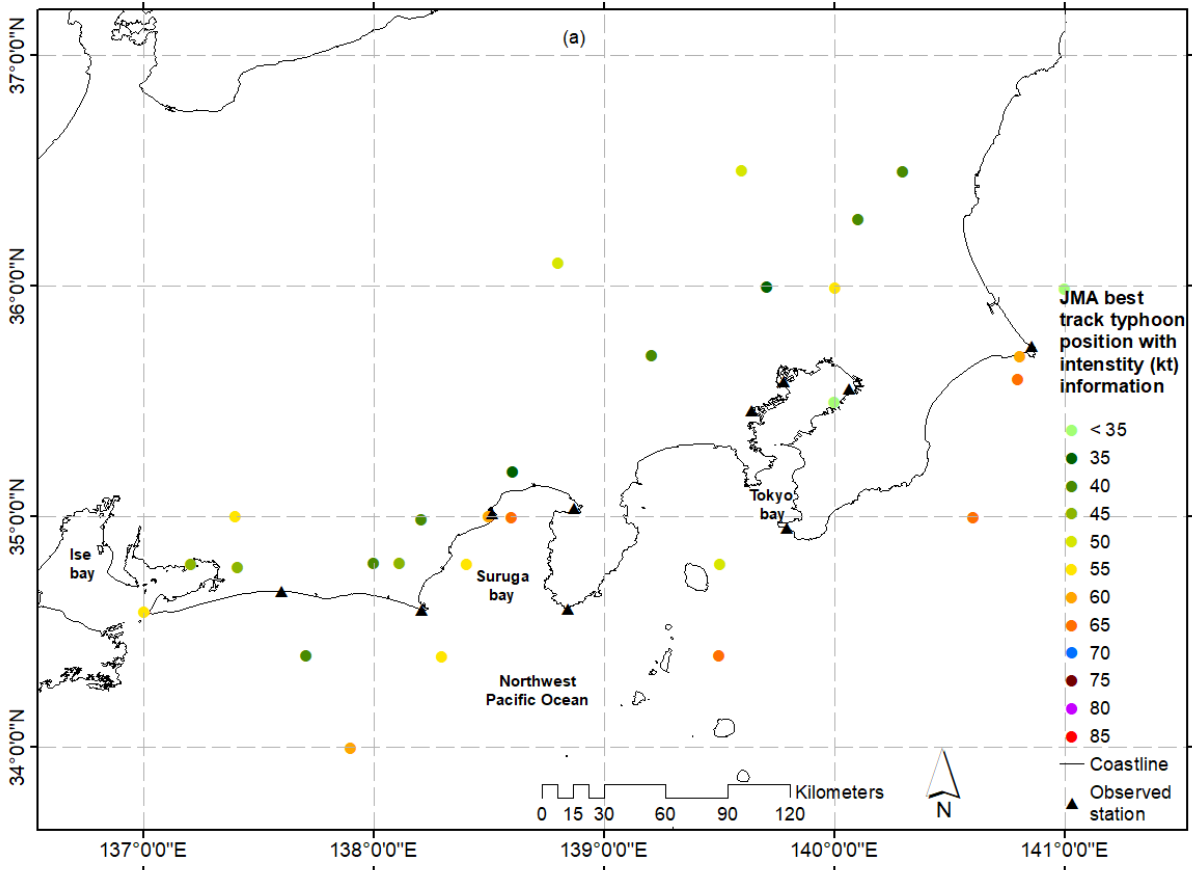


Fig. 9 Comparison between annual mean storm surge heights observed along the Japan Central Coast during 1980-2019 and possible contribution of TC meteorological parameters in SSHPI. See also Table 3.



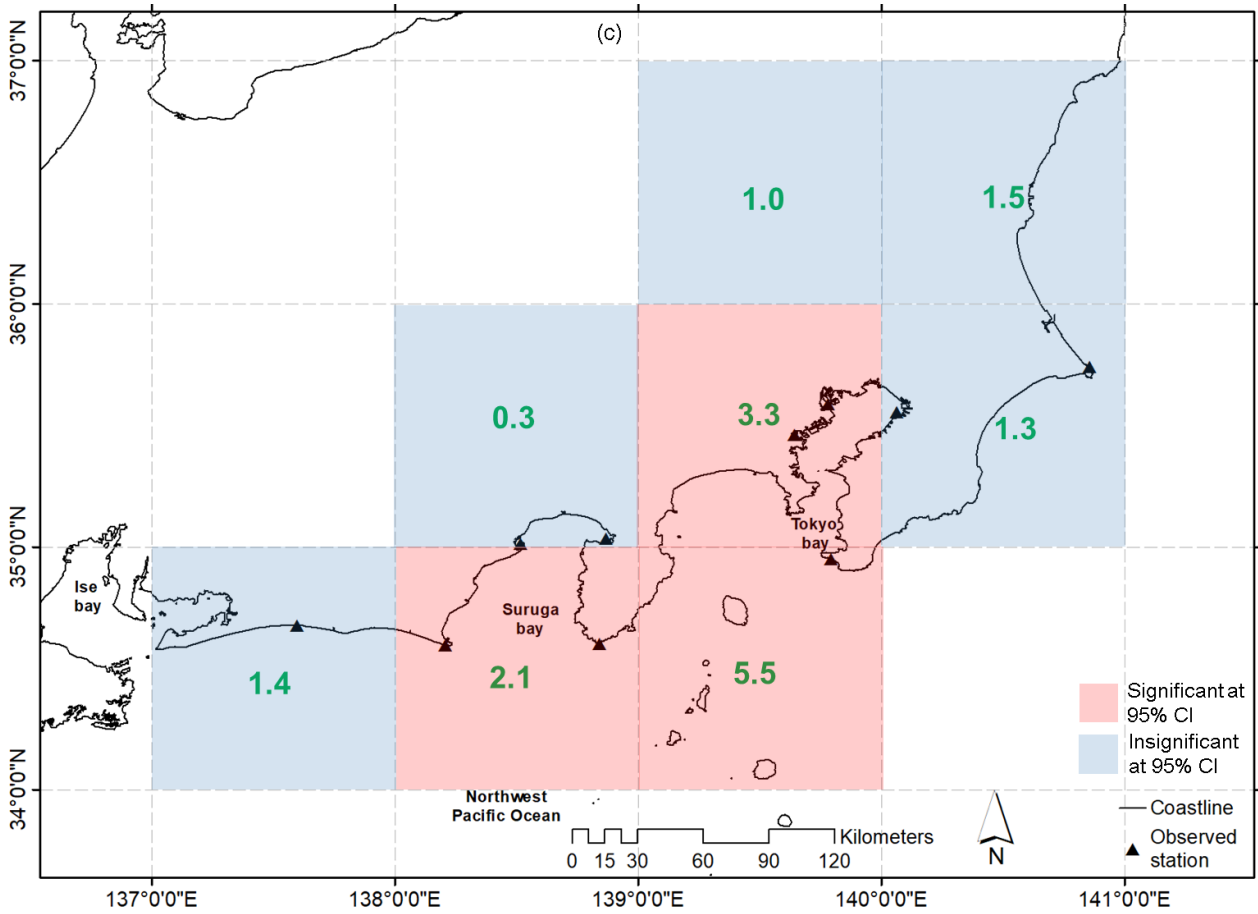


Fig. 10 Landfalling TC six-hourly best track position along with intensity information bounded in latitude by 34°N and 37°N, and longitude by 137°E and 141°E. in (a) 1980-1999; (b) 2000-2019; (c) The change in the landfalling TC activity (the number of TCs central position in 2000-2019 divided by that in 1980-1999; green colored number) in each grid.

List of Tables

Table 1 TC databases and their scope and limitations based on coverage, resolution, and availability.

Table 2 TC meteorological parameter characteristics during landfall time frame between 1980-1999 and 2000-2019, with the p-value for the two-tailed Student's t-test assessing the statistical significance of their difference.

Table 3 Possible contribution of TC meteorological parameters in storm surge variation observed during 1980-2019. The contribution (%) is calculated assuming that only some of the TC meteorological parameters included in SSHPI changed between P1 and P2, while maintaining the other parameters value at their averages from P1.

Table 1 TC databases and their scope and limitations based on coverage, resolution, and availability.

Database	Type	Resolution		Unit	Data range
		Temporal	Spatial		
TC 10 minutes - sustained wind speed	Best track	6 hourly	–	kt	1980–2019
TC size (radius of 50-kt wind)	Best track	6 hourly	–	NM	1980–2019
TC forward speed	Best track	6 hourly	–	Km h ⁻¹	1980–2019
Coastal bathymetry	Gridded bathymetry data	–	500 m	m	34°–36°N, 137°–141°E
Observed storm tide	–	1 hourly	–	cm	1980–2019
Predicted astronomic tide	–	1 hourly	–	cm	1980–2019
Observed storm surge	–	1 hourly	–	cm	1980–2019

Table 2 TC meteorological parameter characteristics during landfall time frame between 1980-1999 and 2000-2019, with the p -value for the two-tailed Student's t -test assessing the statistical significance of their difference.

TC parameter	1980-1999	2000-2019	p -value
Maximum sustained wind speed (kt)	55	64	0.004
Radius of 50-kt wind (NM)	50	65	0.01
Translation speed (km h ⁻¹)	43	41	0.075

Table 3 Possible contribution of TC meteorological parameters in storm surge variation observed during 1980-2019. The contribution (%) is calculated assuming that only some of the TC meteorological parameters included in SSHPI changed between P1 and P2, while maintaining the other parameters value at their averages from P1.

SSHPI components	1980-1999 (P1)	2000-2019 (P2)	Change parameter in P2	Contribution (%)
Wind speed (kt)	55	64	Wind speed	~35
Size (NM)	50	Set to the same value as P1		
Translation speed (km h ⁻¹)	43	Set to the same value as P1		
Wind speed (kt)	55	Set to the same value as P1	Size	~32
Size (NM)	50	66		
Translation speed (km h ⁻¹)	43	Set to the same value as P1		
Wind speed (kt)	55	Set to the same value as P1	Translation speed	~5
Size (NM)	50	Set to the same value as P1		
Translation speed (km h ⁻¹)	43	41		
Wind speed (kt)	55	64	Wind speed and size	~79
Size (NM)	50	66		
Translation speed (km h ⁻¹)	43	Set to the same value as P1		
Wind speed (kt)	55	64	Wind speed, size, and translation speed	~70
Size (NM)	50	66		
Translation speed (km h ⁻¹)	43	41		